



Babeş - Bolyai University
Faculty of Physics



George-Sergiu Mile

**Molecular and electronic structures
of some molecules and molecular complexes
with applications in molecular electronics**

PhD. Thesis Summary

Scientific supervisor:

Prof. dr. Vasile Chiş

Cluj-Napoca

2012

Acknowledgements

I would like to express my gratitude to my supervisor, Professor Dr. Vasile Chiş, for the coordination of my PhD. thesis as I have benefited from his moral support, his entrustment and his intellectual investment in me. We had exchanges of ideas on scientific issues of the greatest importance for the completion of this research. His expertise, accuracy and human and scientific consistency have made a role model for me and I hope that I will be able to follow these qualities in my future.

I thank all members of the thesis jury for the consideration of accepting to judge my work and for giving me valuable insights on the topic. I feel privileged to benefit from their recognized experience and authority in the scientific field.

I want to give some special thanks to our IT engineer Ms. Teodora for her moral and technical support during my research work to PhD. I will always feel attached to her kindness.

I thank my friends and colleagues Lect. Dr. Nicolae Leopold, Mircea, Laci, Sanda, Radu, Nicoleta, Cristi and Camelia for a good and professional collaboration within our research group. There were also pleasant moments spent together in these years of my thesis but the most important gratitude is because they help me many times to express in words what I would rather express in figures and formulas. Many thanks to my friend Dana Sala, who supervised the English version of the thesis and who proof-read the manuscript.

Last but not least I am grateful to my family and friends, first of all to my mother, Cornelia, who has taught me about the greatness of the small things and of the big things, a science which every scientist should master.

The programme “Doctoral studies: through science towards society“, contract POSDRU 6/1.5/S/3 is highly acknowledged for the financial support and for offering the proper framework of the research stages.

Table of contents

INTRODUCTION.....	1
1 THEORY AND METHODOLOGY.....	6
1.1 QUANTUM MECHANICS MODEL.....	7
1.2 HARTREE-FOCK APPROXIMATION	8
1.2.1 <i>Hartree-Fock equations</i>	9
1.2.2 <i>Roothaan-Hall equations</i>	10
1.3 MÖLLER-PLESSET PERTURBATION THEORY.....	11
1.4 DENSITY FUNCTIONAL THEORY.....	14
1.4.1 <i>Hohenberg-Kohn Theorems</i>	15
1.4.2 <i>Kohn-Sham equations</i>	16
1.4.3 <i>Exchange-correlation functionals</i>	19
1.5 DENSITY FUNCTIONAL THEORY WITH DISPERSION CORRECTION.....	26
1.5.1 <i>DFT-D1 and DFT-D2</i>	27
1.5.2 <i>DFT-D3</i>	29
1.5.3 <i>DFT with dispersion correcting potentials</i>	32
1.6 BASIS SETS.....	34
1.7 CALCULATION OF EXCITATION ENERGIES BY TD-DFT	35
1.7.1 <i>Time dependent Kohn-Sham equations</i>	38
1.7.2 <i>Linear response in TD-DFT</i>	39
1.8 CALCULATION OF ABSORPTION AND EMISSION SPECTRA	41
2 VIBRATIONAL AND ELECTRONIC STRUCTURE OF PTCDI AND MELAMINE-PTCDI COMPLEXES	45
2.1 INTRODUCTION	45
2.2 EXPERIMENTAL AND COMPUTATIONAL DETAILS	46
2.3 FT-IR AND RAMAN SPECTRA OF PTCDI.....	47
2.4 VIBRATIONAL SPECTRA OF MELAMINE.....	58
2.5 ADSORPTION OF PTCDI ON SILVER SURFACE.....	61
2.6 THEORETICAL INVESTIGATION OF THE HYDROGEN-BONDED MELAMINE-PTCDI COMPLEXES.....	63
2.7 CONCLUSIONS	70
3 ABSORPTION AND FLUORESCENCE SPECTRA OF PTCDI: AN EXPERIMENTAL AND THEORETICAL STUDY	72
3.1 INTRODUCTION	72
3.2 EXPERIMENTAL AND COMPUTATIONAL DETAILS	74
3.3 ABSORPTION AND FLUORESCENCE SPECTRA	75
3.4 CALCULATED VIBRONIC STRUCTURE OF THE ABSORPTION SPECTRUM OF PTCDI	84
3.5 CONCLUSIONS	93
4 POTENTIAL ENERGY CURVES AND SURFACES FOR PTCDI AND PTCDA OBTAINED BY MP2 AND DISPERSION CORRECTED DFT METHODS.....	95
4.1 COMPUTATIONAL DETAILS.....	97
4.2 BENZENE COMPLEXES AS TEST CASES	99
4.3 POTENTIAL ENERGY CURVES.....	101
4.4 IMPACT OF THE DISPERSION CORRECTION SCHEME	105

4.5	PERFORMANCE OF PBEO FUNCTIONAL	109
4.6	DISPERSION ENERGIES FOR PTCDI AND PTCDA.....	111
4.7	PARTIAL AND FULL OPTIMIZATIONS OF THE PTCDI AND PTCDA DIMERS	112
4.8	CONCLUSIONS	119
5.	POTENTIAL ENERGY SURFACES OF TCNQ AND 4F-TCNQ.....	121
5.1	INTRODUCTION	121
5.2	COMPUTATIONAL AND EXPERIMENTAL DETAILS	123
5.3	RESULTS AND DISCUSSION	124
5.5	CONCLUSIONS	129
	GENERAL CONCLUSIONS	130
	APPENDIX 1	133
	REFERENCES.....	140

Keywords

DFT, TD-DFT, Potential Energy Surfaces, Dispersion Correcting Potentials, FT-IR, FT-Raman, SERS, UV-Vis, PTCDI, PTCDA, TCNQ, 4F-TCNQ

Introduction

The subject addressed in this PhD thesis focuses on a theoretical and experimental study of a series of candidate molecules for molecular electronic devices. Particularly, we are interested in theoretical and spectroscopical characterization of some organic materials possessing useful properties that make them suitable materials for application in nanotechnology for the construction of field effect transistors, organic semiconductor devices, organic photovoltaic cells or organic light emitting diodes.

In the first chapter of the thesis, a general introduction in the field of quantum chemistry is given. Here are presented the methods used in this research, especially the capabilities of the methods suitable for the particular problems studied.

In the second chapter we will report on the molecular and electronic structure of neutral and ionic forms of PTCDI, and on melamine molecule and melamine-PTCDI complexes. Particularly, we are focusing here on vibrational (FT-IR, FT-Raman) spectra of PTCDI and melamine molecules. Theoretical IR spectrum of melamine-3PTCDI complex is discussed in relation with the component molecules of the complex. Hydrogen bonding parameters and interaction energies for melamine-PTCDI complexes with one, two or three PTCDI molecules, as well as dimers formed from melamine and PTCDI molecules are calculated and different possibilities of auto-assembling observed by different groups are also discussed here.

In chapter three, experimental and theoretical results obtained by investigation of the absorption and fluorescence spectra of pure PTCDI compound in three different solvents (Chloroform, DMF and DMSO) are presented and discussed. The absorption spectra were explained by considering both the contributions of monomers as well as aggregated PTCDI molecules. Time dependent DFT (TD-DFT) calculations performed on monomer and dimer models of the molecule explain convincingly the observed experimental features.

Another interest was to explain the impact of the self-organization process of PTCDI molecules on the absorption and emission spectra of PTCDI in the three used solvents. We also tested here the ability of DFT methods with dispersion correcting potentials (DFT-DCP)

for predicting the absorption and emission spectra of PTCDI, as well as their vibronic structures.

In order to achieve a proper understanding of the arrangement of perylenetetracarboxylic derivatives we investigated the diimide and dianhydride prototype dimers in the fourth chapter. Here we report the binding energies and the resulted interplanar distances in the investigated dimers. This is important since these interactions and the resulted arrangements of the monomers in solid-state greatly affect the charge transport by π -conjugated molecules. For this investigation we used correlated calculations which are essential for describing dispersion interactions. Potential energy curves along the interplanar coordinate have been derived for the dimers of two perylene derivatives (PTCDI and PTCD A) by using MP2 and dispersion corrected DFT (DFT-D) methods

Because the study of molecular clusters is considerably facilitated by the use of an analytical function, the calculated potential energy curves at different levels of theory have been fitted to a modified Morse, Murrell-Sorbie, Buckingham or Lennard-Jones potential and then equilibrium distances and interaction energies were extracted. The effects of the geometrical perturbations (displacements and rotations) from face-to face stacked structures on the stability of the two kinds of dimers (PTCDI and PTCD A) were also studied.

Finally, chapter five present the results obtained by the investigation of the potential energy surfaces of 7,7,8,8-tetracyano-quinodimethane (TCNQ) and its fluorinated analogue 4F-TCNQ. Local minima as well as the global minimum on the potential energy surfaces of the two dimers have been obtained at B3LYP-D2/6-31G(d) level of theory. Both, rigid and relaxed potential energy surfaces have been calculated on suitable grids and the fully optimized dimers were obtained starting from the geometries corresponding to the global minima detected on the PESs of the two dimers.

2 Vibrational and electronic structure of PTCDI and Melamine-PTCDI complexes

2.1 Introduction

Perylene derivatives received great scientific interest in the last years due to their potential applications in molecular electronics. Particularly, 3,4,9,10-perylene-tetracarboxylicdiimide (PTCDI) (see Fig.2.1) and the anhydride analogue (PTCDA) were the subject of studies aiming to elucidate their absorption mechanism on different substrates

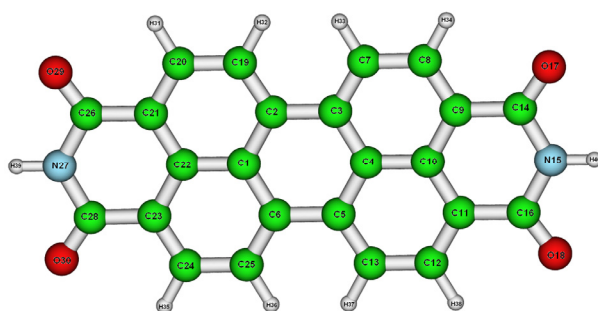


Fig. 2.1 B3LYP/6-31G(d) optimized structure of PTCDI molecule

[Ant91, Zah04, Hau05, Sal06, Kaa07]. Recent studies are reported on the hydrogen-bonding guided assembling by co-adsorption of PTCDI and melamine (1,3,5-triazine-2,4,6-triamine) on silver terminated silicon [The03] or gold surfaces [Sil07]. These studies are focused on self-assembly technique able to order fullerenes on different surfaces. Moreover, being molecules with reversible redox reactions, PTCDI molecule or its derivatives have found very promising applications in silicon-based microelectronics, particularly for the construction of field effect transistors. Tao and coworkers demonstrated experimentally that the current through PTCDI can be reversible varied and controlled over three orders of magnitude by varying the gate voltage [Li06]. Recent research suggests also that PTCDI derivatives are one of a few classes of molecules that show typical n-type characteristics, besides their thermal and photo-stability [Dat06].

A major challenge for nanotechnology and nano-engineering is to control molecular ordering; one very convenient way for this is the self-assembly process of different nanoblocks on atomically well-defined surfaces or the exploiting of intermolecular interactions by mixing different molecular species in order to form extended networks [Rui06, Per06]. In this way, the properties of the resulting supramolecular architectures can

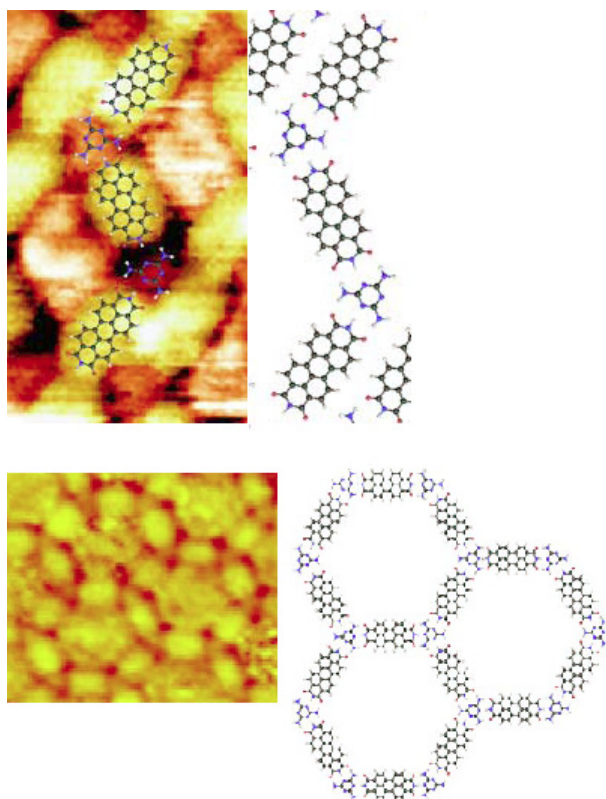


Fig.2.2 Z-shaped and honeycomb arrangements of melamine-PTCDI complexes on Au111 surfaces (adapted from [Sil07])

be tailored by modifying the functionality and structure of the molecular building blocks [Sil08]. Actually, the present study has been motivated by the work of Silly *et al.* [Sil07] who were able to form different supramolecular networks by changing the post-annealing temperature after molecular co-deposition of melamine and PTCDI on Au111 (Fig.2.2).

In this work we will report on the molecular and electronic structure of neutral and ionic forms of PTCDI, and on melamine and melamine-PTCDI complexes. Particularly, we are focusing here on vibrational spectra of PTCDI and melamine, hydrogen bonding

parameters and interaction energies of the melamine-PTCDI complexes [Chi09, Mil09]. Finally, different possibilities of self-assembling of PTCDI molecules are discussed in relation with experimental results obtained by Silly *et al.* [Sil07].

2.2 FT-IR and Raman spectra of PTCDI

PTCDI is a planar molecule belonging to D_{2h} symmetry point group. It has 114 vibrational normal modes, 54 of them are Raman active ($20A_g+7B_{1g}+11B_{2g}+19B_{3g}$), 49 are IR active ($19B_{1u}+19B_{2u}+11B_{3u}$), while 8 modes of A_u symmetry are silent.

Having an inversion center, the IR active modes and Raman inactive and vice versa. As can be seen in Table 2.1, the calculations predict very well the IR/Raman activity/inactivity of the normal modes.

The most intense experimental IR/ATR bands of the PTCDI in the high wave number region ($>1000\text{cm}^{-1}$) are those corresponding to C=O stretching vibrations (1684cm^{-1} – symmetric stretch and 1671cm^{-1} – asymmetric stretch), CC stretchings alone or coupled

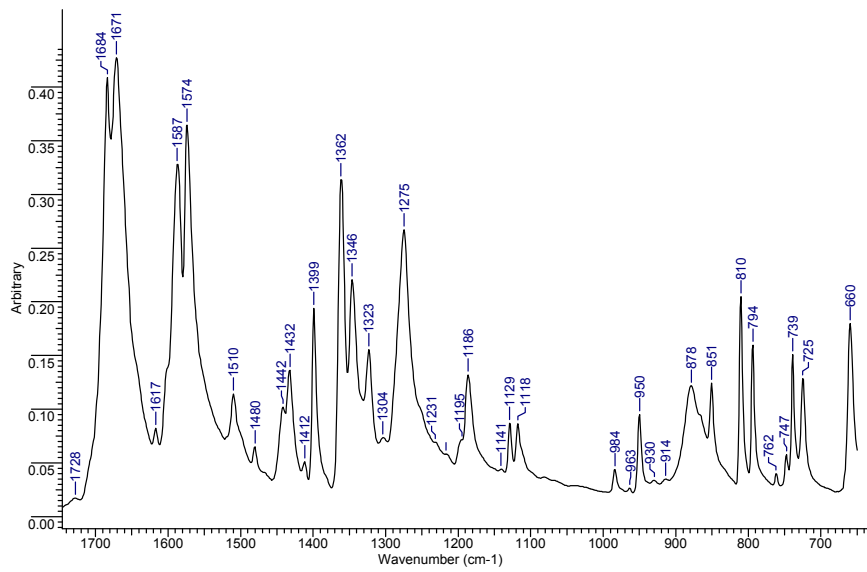


Fig. 2.3 a) FT-IR/ATR spectrum of powder PTCDI at room temperature in the 650-1750 cm^{-1} region

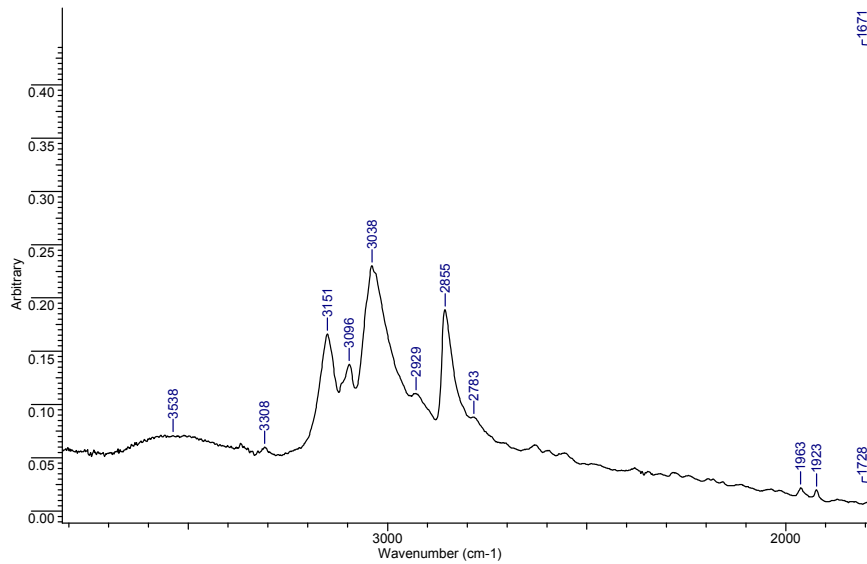


Fig. 2.3 b) FT-IR/ATR spectrum of powder PTCDI at room temperature in the high wavenumber region

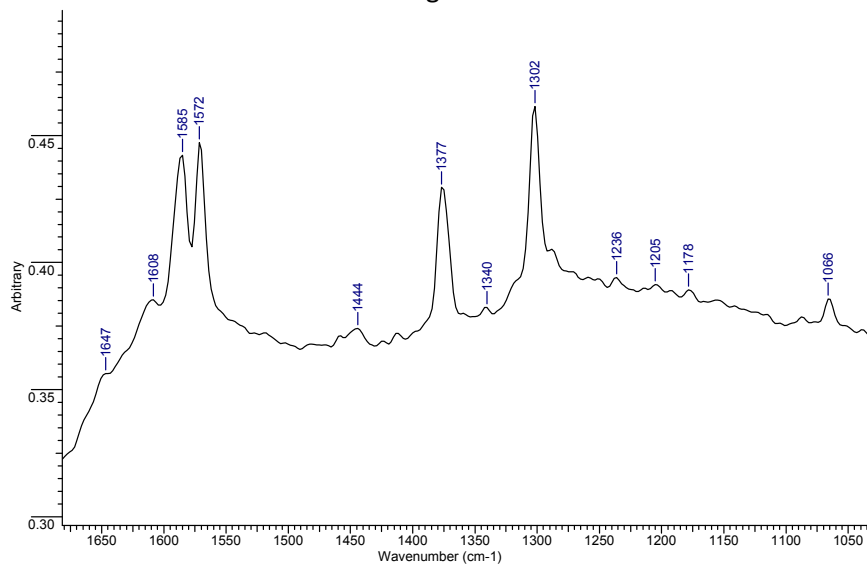


Fig. 2.3 c) FT-Raman spectrum of powder PTCDI at room temperature in the 1000-1700 cm^{-1} region

Table 2.1 B3LYP/6-31G(d) calculated and experimental vibrational spectra for PTCDI molecule

Index	Calculated				Experimental					Assignments
	Symm.	wave number	I[%]	A[%]	ATR	ATR int. [%]	IR	IR int. [%]	Raman	
1	AG	550	0.00	2.13					551	lateral stretch whole molecule
2	AG	656	0.00	0.62					654	central ring stretch
3	B1U	667	5.00	0.00	660	40.48	660	13.50		$\delta(\text{CCC})$
4	B1U	811	3.42	0.00	810	47.62	811	48.17		ip rings deformation
5	B1U	966	3.34	0.00	950	21.43	950	29.67		inner rings breathing
6	AG	1042	0.00	8.83					1066	$\delta(\text{CH})$ +ip rings def.
7	B3G	1166	0.00	0.07					1178	$\delta(\text{CH})$
8	B3G	1231	0.00	1.62					1236	$\nu(\text{CN})+\delta(\text{NH})+\nu(\text{CC})$
9	B2U	1247	23.55	0.00	1275	61.90	1277	63.67		$\nu(\text{CN})+\delta(\text{NH})+\nu(\text{CC})$
10	AG	1257	0.00	8.03					1285	$\delta(\text{CH})+\nu(\text{CC})$
11	AG	1290	0.00	61.01					1302	central ring stretch+ $\delta(\text{CH})$
12	AG	1351	0.0	22.31					1340	$\nu(\text{CN})+\nu(\text{CC})+\delta(\text{CH})$
13	AG	1367	0.00	6.99					1377	$\nu(\text{CN})+\delta(\text{CH})$
14	B2U	1368	3.24	0.00	1362	73.81	1360	82.40		$\delta(\text{NH})$
15	B1U	1380	5.51	0.00	1399	45.24	1399	55.17		$\nu(\text{CC})+\delta(\text{CH})$
16	B3G	1444	0.00	1.02					1444	$\nu(\text{CC})$ inner rings
17	AG	1554	0.00	100.00					1572	$\nu(\text{CC})+\delta(\text{CH})$
18	AG	1576	0.00	56.69					1585	$\nu(\text{CC})$
19	B1U	1582	65.46	0.00	1587	76.19	1585	83.00		$\nu(\text{CC})$
20	B2U	1717	96.29	0.00	1671	100.00	1670	100.00		$\nu_{\text{as}}(\text{CO})$
21	B1U	1718	100.00	0.00	1684	95.24	1688	97.20		$\nu_{\text{s}}(\text{CO})$

with CH in plane bendings (1587, 1574 and 1399 cm^{-1}), NH in plane bending at 1362 cm^{-1} , CN symmetric stretching coupled with CC stretchings and CH in plane bendings (1346 cm^{-1}) and CN asymmetric stretchings coupled with CC stretchings and CH in plane bendings.

All the bands mentioned in table 2.1 have B_u symmetry while the calculated normal modes with appreciable Raman activity have A_g symmetry and the results are in good agreement with those reported by Rodriguez Lloret *et al.* [Llo98] and by Aroca *et al.* [Aro97].

2.3 Theoretical investigation of the hydrogen-bonded melamine-PTCDI complexes

Molecular complexes formed by one melamine with one, two and three PTCDI molecules have been optimized at B3LYP/6-31G(d) level of theory. C_{2v} and D_{3h} symmetries were adopted for the first two and the third complex, respectively.

The calculated hydrogen bonding parameters (NH, CO, N...N, N...O and NHO angle) for PTCDI and the three investigated melamine-PTCDI complexes are given in Table 2.2. A

significant increase in the NH bond is noted going from the PTCDI molecule alone to the melamine-PTCDI complexes, accompanied by a lengthening of CO and N...N and C...O bonds.

Table 2.2 B3LYP/6-31G(d) calculated hydrogen bonding parameters for PTCDI in different complexes (bond lengths in Å and angles in degrees)

	NH	CO	N...N	N...O	<NH...O
PTCDI	1.015	1.221	-	-	-
Melamine-1PTCDI	1.049	1.230	2.927	2.970	176.4
Melamine-2PTCDI	1.049	1.230	2.938	2.964/2.992	178.0
Melamine-3PTCDI	1.048	1.229	2.950	2.983	179.1

The calculated hydrogen bonding parameters suggest an important stabilization of the melamine-3PTCDI complexes (see Fig. 2.) due to the three strong hydrogen bonds between each pair of PTCDI and melamine molecules. It is worth mentioning that for this complex, the calculated center-to-center spacing of PTCDI-melamine pair (10.018 Å) is in excellent agreement with the measured separation of 9.980 Å obtain by Theobald et al. [The03].

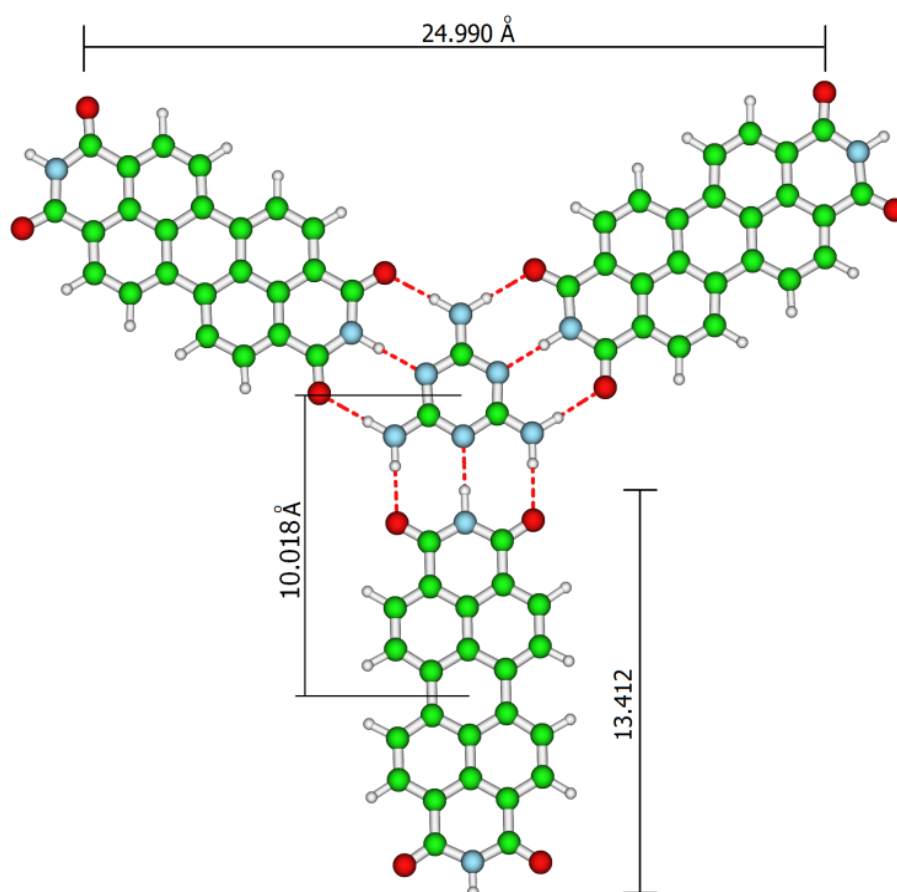


Fig. 2.3 B3LYP/6-31G optimized geometry of the melamine-3PTCDI molecular complex

The stabilization energies in the melamine-PTCDI complexes for 1 PTCDI molecules, i.e., total interaction energy divided by the number of PTCDI molecules in the corresponding complex are -14.91, -14.53 and -14.04 kcal/mol

2.4 Conclusions

Vibrational IR and Raman spectra of PTCDI and melamine molecules were recorded and safely assigned based on B3LYP/6-31G(d) calculations by considering both the frequency sequence and intensity pattern of the experimental and theoretical spectra. The largest discrepancy between experiment and theory for the IR spectrum of PTCDI was found for the carbonyl group stretchings and it is attributed to the hydrogen bonding interaction between neighboring molecules in solid state.

The calculated hydrogen bonding parameters for melamine and its complexes with PTCDI molecules show an important stabilization of the complexes formed from melamine and one, two or three PTCDI molecules due to three strong hydrogen bonds. Calculated stabilization energies for melamine-PTCDI complexes and melamine and PTCDI dimers suggest that melamine-PTCDI interaction is more preferred than melamine-melamine or PTCDI-PTCDI interactions. However, the later interactions, with similar characteristic energies and larger than 9 kcal/mol can play an important role when these molecules are (co)deposited on different surfaces. Moreover, the small calculated difference between the interaction energies corresponding to the three melamine-PTCDI complexes is an indicative of the ability of the melamine molecule to form stable complexes regardless of the number of PTCDI molecules.

3 Absorption and fluorescence spectra of PTCDI: an experimental and theoretical study

3.1 Introduction

For applications in material science, π -conjugated molecules with charge and energy transport properties like perylenebis-imides possesses very favorable properties such as intense photoluminescence, making them particularly interesting for applications in organic solar cells, organic light emitting diodes and other opto-electronic devices [Zha09, Wan09]. Applications of these dyes are dependent on their absorption properties, charge carriers and exciton mobilities [Sei06] because these properties are affected by the electronic interactions between the monomers in the aggregated states and their spatial arrangements. While the packing geometry in solid state can be easily obtained from X-ray diffraction studies, however, the same information is not easily available for self-assembled aggregates in solution.

UV-Vis absorption spectra are sensitive to inter-chromophore distance and orientation and have been widely used to study π - π stacking of perylene derivatives dyes [Yan05]. For instance, self-assembling of PTCDI derivatives into one-dimensional structures is a processes governed by a delicate balance between molecular stacking and solubility [Bal05, Fer06]. The twisting between PTCDI monomers in supramolecular units leads to weaker π - π interaction between the molecules and consequently, to a distortion of the packing from the face-to-face conformation. This fact has as a result a red-shifted emission of the self-assembled crystals [Zha09].

To the best of our knowledge, only a few studies [Gus97, Cla07] are reported on the vibronic structure of PTCDI itself; however these studies used common DFT methods for calculating the absorption spectrum. Moreover, Clarck and collaborators [Cla07] used the optimized triplet excited state of PTCDI, instead of the singlet excited state, for obtaining the vibronic structure of the absorption spectrum. For these reasons we decided to investigate the absorption and fluorescence spectra of pure PTCDI compound in three different solvents (Chloroform, DMF and DMSO) and to test the ability of DFT-DCP methods for predicting the absorption and emission spectra of PTCDI, as well as the vibronic structure

of its absorption spectrum [Olt11]. Another interest is to explain the impact of the self-organization process of PTCDI molecules on the absorption and emission spectra of PTCDI in the three solvents: chloroform, DMF and DMSO.

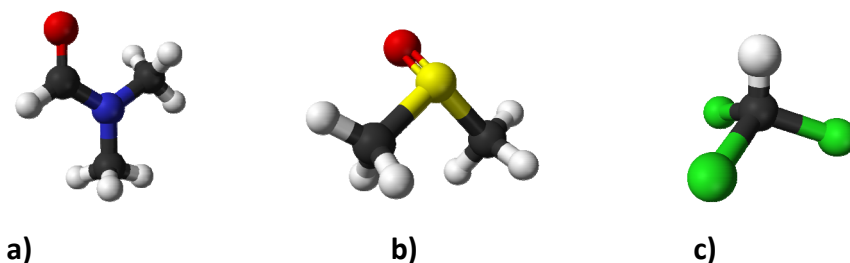


Fig. 3.1 Molecular structures of the solvents used for measuring the absorption spectra of PTCDI: DMF (a), DMSO (b) and chloroform (c)

3.2 Absorption and fluorescence spectra

The UV-Vis absorption and fluorescence spectra of PTCDI in chloroform solution are given in Fig.3.2, while absorption spectra in DMF and DMSO solutions are presented in Fig. 3.3 and 3.4. As shown in Fig.3.2, a well-defined vibronic structure is observed for the $S_0 \rightarrow S_1$ transition in chloroform solution in absorption as well as in the mirror image fluorescence spectra, the peak maxima being located at 526 and 540 nm in the absorption and emission spectra, respectively. Such a small value of the Stokes shift, 14 nm (0.06 eV) is expected if the structural parameters of the excited state geometry are only slightly affected.

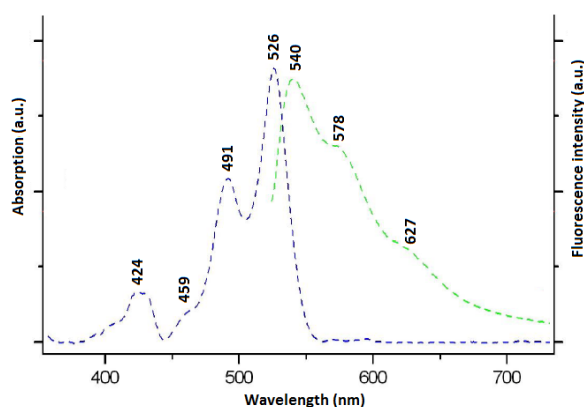


Fig. 3.2 UV-Vis absorption and fluorescence spectra of PTCDI in Chloroform

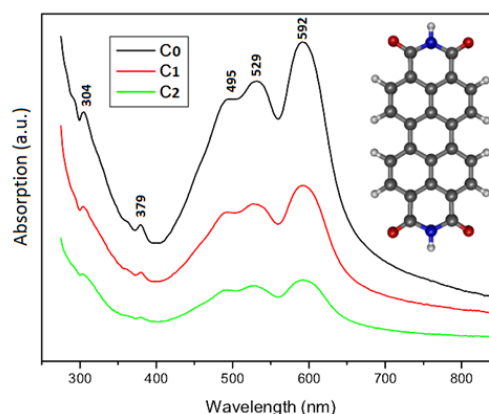


Fig. 3.3 UV-Vis absorption spectrum of PTCDI in dimethylformamide at three different concentrations

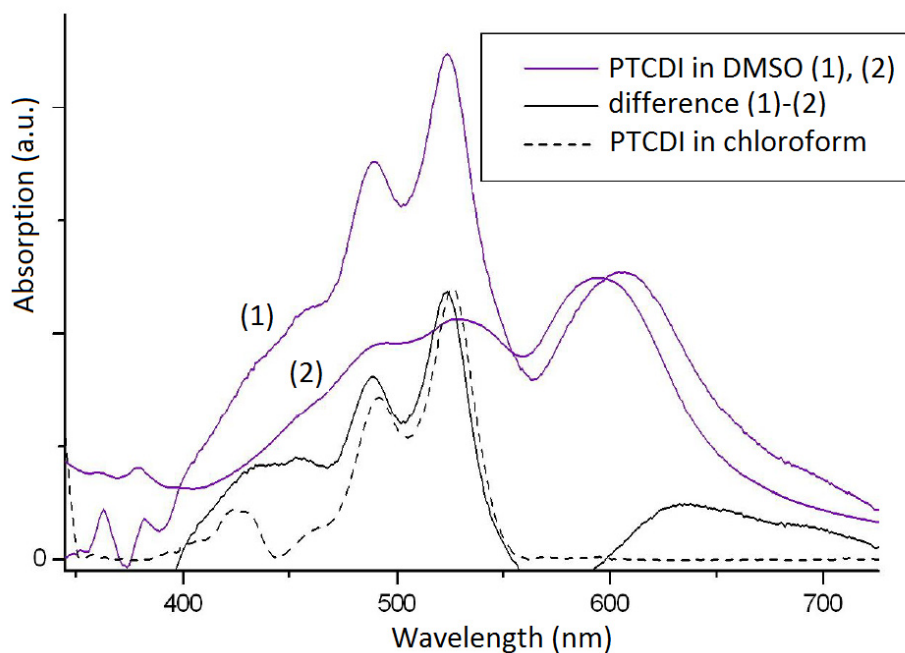


Fig. 3.4 Absorption spectra of PTCDI in DMSO at two different concentrations: low concentration – curve (1) and CO concentration – curve (2). Absorption spectrum in Chloroform is added for comparison purposes.

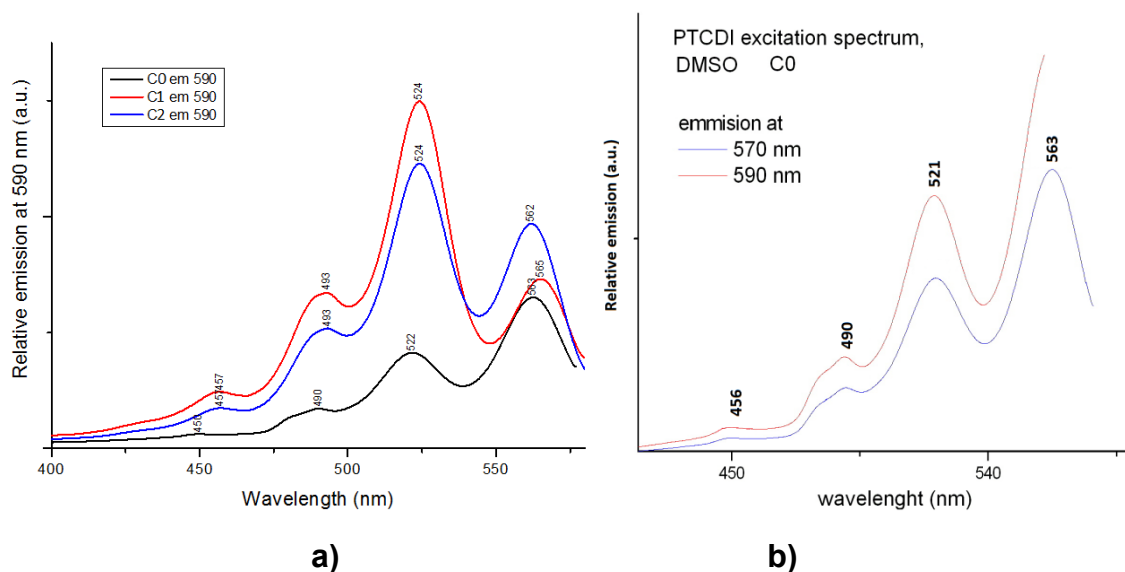


Fig. 3.5 Excitation spectra of PTCDI in: **a)** DMF at three different concentrations with the emission monitored at 590 nm **b)** DMSO (C0 solution), with the emission monitored at 570 and 590 nm.

Contrary to the chloroform solution, as shown in Fig. 3.3 and 3.4, the vibronic structure is not well resolved for the other two solvents. Moreover, compared to chloroform, in DMF and DMSO solutions, a supplementary peak appears in the absorption spectra at 592 and 598 nm for DMF and DMSO, respectively. This band is assigned to the

aggregated PTCDI molecules. Similar bands were identified for N,N'-di(nonyldecyl)-PTCDI poor solvents [Bal06] or for PTCDI derivatives in methanol and methylcyclohexane by decreasing the temperature [Yan08].

The absorption spectrum of PTCDI in DMF shown in Fig. 3.5 was recorded for three different concentrations; C0 is the concentration obtained as a direct result of the preparation, C1 and C2 mean the ratios C0/DMFA 1:2 and C0/DMFA 1:3, respectively.

The difference between the curves (1) and (2) (normalized such that the band due to aggregates has the same intensity) gives a very similar spectrum to that observed in chloroform, confirming that in less concentrated DMSO solution a larger concentration of free (un-assembled) PTCDI molecules exist which absorb almost at the same wavelengths.

Comparing the three used solvents it is clear that the E0-0 peak in the vibronic progression of S0->S1 transition which dominates the spectra are affected by the dielectric constant of the solvent, particularly in the case of DMSO. Thus, the E0-0 energies are 2.36 eV (526 nm) for chloroform, 2.34 eV (529 nm) for DMF and 2.30 eV (538 nm) for DMSO.

Table 3.1 TD PBE0-DCP/6-31+G(d,p) calculated excited states of PTCDI monomer in gas phase and in dimethyl formamide. For each singlet state main electron configurations are displayed where absolute values of their coefficients are shown in parentheses. The most intense calculated electronic transitions are highlighted in bold face.

No.	Configuration	E(nm)	f
PTCDI monomer(gas-phase)			
1	HOMO→LUMO (0.70)	507.6	0.654
2	HOMO-4 → LUMO (0.66) HOMO→LUMO+4 (0.21)	337.8	0.054
3	HOMO→LUMO+4 (0.16)	296.5	0.067
PTCDI monomer (dimethylformamide)			
1	HOMO→LUMO (0.70)	537.3	0.864
2	HOMO-2 → LUMO (0.67) HOMO→LUMO+4 (0.17)	346.3	0.127
3	HOMO→LUMO+4 (0.17)	283.6	0.067

TD-DFT calculations (see Table 3.1) reveal that $S_0 \rightarrow S_1$ transition for PTCDI monomer in gas-phase has oscillator strength of 0.654 and corresponds to a HOMO-LUMO excitation (see Fig.3. 6).

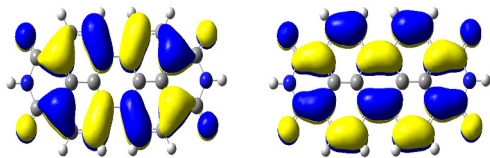


Fig.3.6 HOMO (left) and LUMO (right) of PTCDI

526 nm this work).

As shown in Table 3.1 the calculated energies of the allowed transitions for the gas-phase PTCDI is 507 nm and it is in a satisfactory agreement with the energies of the measured absorption bands obtained on PTCDI dissolved in DMF (526 nm), DMSO (538 nm) and chloroform (520 nm [Gus97],

3.3 Calculated vibronic structure of the absorption spectrum of PTCDI

Vibronic transitions are those transitions which involve a change in both the electronic and vibrational quantum numbers of a molecular entity, as opposed to purely electronic or vibrational transitions. In other words, the transition occurs between two states, involving a change in both electronic and vibrational energy [IUP97]. The vibronic structure in the UV-Vis spectra of PTCDI is due to the simultaneous excitation of the electronic transition and one (or more) vibrational modes, the coupling between the two types of excitations being determined by the Franck-Condon factors. These factors are in turn determined by the square of the overlap integral of the vibrational wave functions $\psi_{\text{vib}}(v_i)$ and $\psi_{\text{vib}}(v_f)$ in the ground and excited electronic states. Large Franck-Condon factors are expected only for totally symmetric vibrations that should be elongated under the dipole allowed transitions.

As shown in Fig.3.2, the UV-Vis absorption spectrum shows two distinct bands located at 526 and 491 nm, and a shoulder at 459 nm. The difference between the positions of the first and second band is 1355 cm^{-1} , while between the second and the third (shoulder) it is 1420 cm^{-1} , comparable to the energy of vibrational modes involving CC stretches in PTCDI. Similar spacings between the peaks forming the vibronic structure are observed for the spectra recorded in DMF and DMSO. We assigned these peaks to the vibrational structure of the absorption band corresponding to $S_0 \rightarrow S_1$ electronic transition.

In Fig.3.7 the completely optimized gas-phase geometries of PTCDI in both, ground and first excited states are presented. As for the ground state, the excited state geometries remain planar, with an almost D_{2h} symmetry. A slight reduction of the CC bonds parallel to the long axis of the molecule (the bonds between the two naphthalene moieties), but also

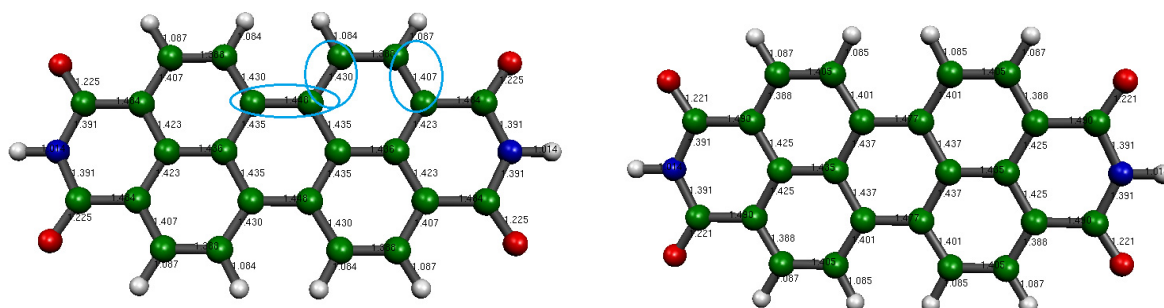


Fig. 3.7. Optimized bond lengths for the ground state (left) and first excited state (right) of PTCDI in gas phase at PBE0-DCP/6-31+G(d,p) level of theory for some of the diagonal bonds is observed for the geometry of the first excited state. The most affected bonds are those marked by ellipses and their symmetry equivalent partners.

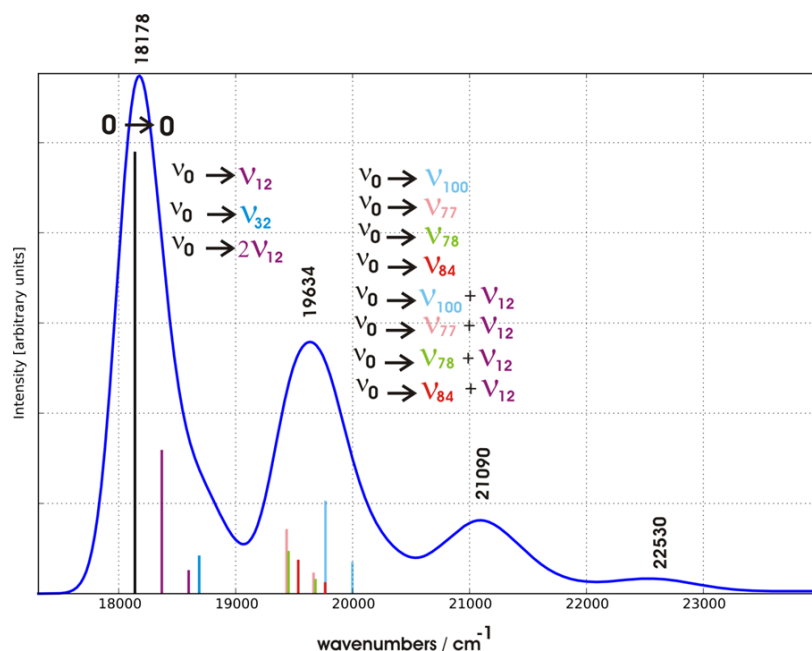


Fig. 3.8. PBE0-DCP/6-31+G(d,p) calculated absorption spectrum of PTCDI monomer in gas phase (excitation to the first electronic excited state). The stick lines refer to the individual vibronic transitions (the lengths of the bars indicate the oscillator strength).

The pure electronic transition $\langle 0|0\rangle$ is situated at 18138 cm^{-1} (see Fig.3.8). A second intense line of the first peak is the transition $\langle 0||12^1\rangle$ which correspond in the vibronic spectrum to a transition from the fundamental vibrational mode of electronic fundamental state S_0 to the v_{12} vibrational mode in the first (S_1) excited state. This line has about 1/3 of

the intensity of the $\langle 0|0\rangle$ transition line and is shifted by 230 cm^{-1} from the corresponding line. This shift has a direct implication to the Half-Width at Half-Maximum of the first band which is about 260 cm^{-1} . Thus this transition is observed also in the rest of the spectrum but with a reduced intensity and in a combination with other vibrational modes such as ν_{77} , ν_{78} , ν_{84} and ν_{100} vibrations of the S_1 state.

For the second peak, the most important transitions from the ground electronic state S_0 to the ν_{100} , ν_{77} , ν_{78} and ν_{84} vibrational modes in the excited state S_1 or in the combination of these four modes with the ν_{12} mode. The combinations are generally three times less intense than the transitions between the fundamental state and the ν_{100} , ν_{77} , ν_{78} and ν_{84} vibrational levels of the excited S_1 state.

3.4 Conclusions

Absorption and emission spectra of PTCDI have been investigated in three solvents (chloroform, DMF and DMSO). For chloroform no signature of the aggregated PTCDI molecules was observed in the experimental spectrum. For DMF and DMSO the absorption band seen at 592 and 598 nm, respectively, represents a clear evidence for the formation of the aggregates of PTCDI molecules. By TD-DFT calculations we were able to confirm this assumption using a simple dimer model. The first excited state has B_{1u} symmetry and it is a result of a HOMO \rightarrow LUMO transition. The second excited state of PTCDI is a result of the HOMO-4 \rightarrow LUMO transition and has B_{2u} symmetry.

The geometry of the excited state remains planar but, with respect to the ground state geometry it is slightly shortened along the long axis of the molecule. The most affected bonds are those connecting the two naphthalene moieties.

Excitation energies have been calculated both in the framework of TD-DFT formalism as well as by using the Franck-Condon approximation. A clear improvement is observed between the experimental and computed excitation energies within the FC approximation.

The vibronic structure of the absorption spectrum of PTCDI was explained on the basis of FC approximations which predicted that five normal vibrational modes and their combination bands contribute significantly to the observed vibronic progression observed in the experimental spectrum. Thus, besides the 0-0 transition, the first vibronic peak contains an important contribution due to the excitation of ν_{12} vibrational mode of PTCDI. The second peak is mainly due to the excitation of ν_{100} , ν_{77} , ν_{78} and ν_{84} modes.

4 Potential energy curves and surfaces for PTCDI and PTCDA obtained by MP2 and dispersion corrected DFT methods

4.1 Benzene complexes as test cases

Since one of the objectives of this work is related to the ability of DCPs for giving accurate binding energies and PECs for the two perylene derivatives we tested firstly this method on two different systems (S and T-shaped benzene dimers see Fig.4.1). Thus, we fully optimized the benzene monomer with D_{6h} symmetry and T-shaped benzene dimer with C_{2v} symmetry using the PBE0-DCP/BS2 method. The calculated binding energies 9.85 kJ/mol (without BSSE correction) and the calculated distance between the centers of mass of the two monomers is 5.002 Å, in excellent quantitative agreement with the available experimental data [Gro87,Aru93] (10.04 kJ/mol, 4.96 Å)

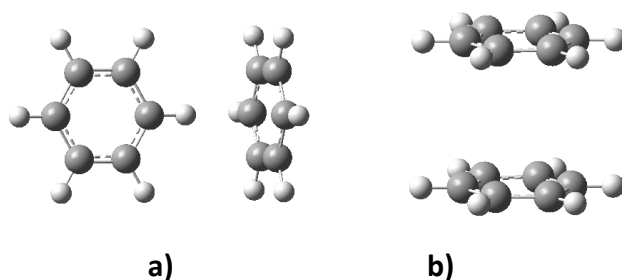


Fig. 4.1 Model dimers used for testing the DFT-DCP method for predicting geometry and interactions energies: a) T-shaped benzene dimer; b) parallel benzene dimer;

For the sandwich configuration of the fully optimized benzene dimer at PBE0-DCP/BS2 level of theory we obtained a binding energy of 5.80 kJ/mol, with an equilibrium distance between the planes of the monomers of 3.816 Å. The bond distances in the optimized dimer are: $R_{CC} = 1.402$ Å and $R_{CH} = 1.088$ Å. Once again we note the excellent agreement between the present results and those calculated at (much more laborious) BSSE-corrected CCSD(T)/aug-cc-pVQZ level of theory [Sin04] ($D_e=5.56$ kJ/mol, $R_e=4.0$ Å).

4.2 Potential energy curves.

The calculated PECs were fitted with the modified Morse (mM), general Lennard-Jones (LJ), Murrell-Sorbie (MS) and Buckingham potentials given below [Sto97]:

$$V_{mM}(r) = D_e \left[1 - \left(1 - \exp(-\alpha(r - R_e)) \right)^2 \right]$$

$$V_{LJ}(r) = \left(\frac{a}{r} \right)^b - \left(\frac{c}{r} \right)^d \quad (4.1)$$

$$V_{MS}(r) = D_e [1 + \alpha_1(r - R_e) + \alpha_2(r - R_e)^2 + \alpha_3(r - R_e)^3] \cdot \exp[-\alpha_1(r - R_e)]$$

$$V_B(r) = a \cdot \exp(-br) - \frac{c}{r^6}$$

where D_e and R_e are the well depth and equilibrium distance, respectively.

The above equations are used directly for the parameterization of interaction potentials, treating each monomer as one interacting point [Lil06]. Binding energies (D_e) and intermolecular equilibrium distances (R_e) for the two types of stacked dimers, as obtained by fitting the calculated data to the four potentials are collected in Tables 4.1 and 4.2.

Fig. 4.2 and 4.3 show the binding energy curves for PTCDI and PTCDA, respectively, obtained using MP2, B3LYP-D, B97-D, PBE0-D, PBE0-DCP and B971-DCP3 approaches, with CP correction for BSSE and fitted to a Murrell-Sorbie APEF [Olt12].

As shown in Tables 4.1 and 4.2, all the computational methods predict weaker binding in PTCDA than in PTCDI dimer. Based on the MS fitted PECs, B3LYP-D3/BS1, B97-D3/BS1 and PBE0-D3/BS2 approaches provide larger binding energies for PTCDI by 136, 122 and 128 meV, respectively. PBE0-DCP (BSSE uncorrected) method still predict a tighter PTCDI dimer than in the case of the anhydride analogue but the difference in binding energies is significantly lower, e.g. between 70 and 80 meV with respect to the MP2 and other DFT-D methods.

It is also observed that the BSSE has a great impact on both binding energies and equilibrium distances. While the non CP-corrected MP2 calculated D_e for PTCDI varies, depending on the fitting potential, between -1.11 eV and -1.162 eV, the BSSE corrected D_e values are almost half of the uncorrected ones. This lowering of D_e 's is accompanied by a significant increase of the intermonomer distance (see Table 4.1). For PTCDA, the BSSE uncorrected and corrected MP2 binding energies are consistently smaller than for PTCDI, regardless of the fitting potential.

Table 4.1 Calculated binding energies (in eV) and equilibrium intermolecular distances (in Å) for the stacked PTCDI dimer at different levels of theory^a.

PTCDI								
Method	$-D_e(\text{eV})$				$R_e(\text{Å})$			
	mM	LJ	MS	B	mM	LJ	MS	B
MP2/6-31G(d)	0.639 (1.114)	0.642 (1.162)	0.699 (1.151)	0.667 (1.160)	3.647 (3.462)	3.640 (3.402)	3.708 (3.500)	3.662 (3.436)
B3LYP-D3/6-31G(d)	0.808 (1.099)	0.799 (1.115)	0.799 (1.104)	0.802 (1.094)	3.647 (3.542)	3.600 (3.507)	3.626 (3.540)	3.633 (3.527)
B97-D3/6-31G(d)	0.886 (1.161)	0.874 (1.174)	0.868 (1.160)	0.883 (1.160)	3.645 (3.551)	3.604 (3.513)	3.629 (3.541)	3.640 (3.538)
PBE0-D3/6-31G(d)	0.679 (0.901)	0.606 (0.910)	0.668 (0.902)	0.672 (0.895)	3.715 (3.613)	3.728 (3.568)	3.699 (3.621)	3.703 (3.601)
PBE0-D3/6-31+G(d,p)	0.660 (0.865)	0.647 (0.854)	0.649 (0.851)	0.653 (0.862)	3.722 (3.697)	3.676 (3.644)	3.709 (3.676)	3.711 (3.684)
PBE0-DCP/6-31+G(d,p)	(0.667)	(0.688)	(0.677)	(0.653)	(3.579)	(3.542)	(3.592)	(3.566)

Table 4.2 Calculated binding energies (in eV) and equilibrium intermolecular distances (in Å) for the stacked PTCDA dimer at different levels of theory^a.

PTCDA								
Method	$-D_e(\text{eV})$				$R_e(\text{Å})$			
	mM	LJ	MS	B	mM	LJ	MS	B
MP2/6-31G(d)	0.553 (1.028)	0.554 (1.047)	0.555 (1.027)	0.549 (1.025)	3.664 (3.437)	3.620 (3.408)	3.659 (3.473)	3.654 (3.420)
B3LYP-D3/6-31G(d)	0.665 (0.946)	0.666 (0.969)	0.663 (0.953)	0.656 (0.937)	3.642 (3.533)	3.597 (3.505)	3.637 (3.543)	3.630 (3.519)
B97-D3/6-31G(d)	0.758 (1.021)	0.753 (1.039)	0.746 (1.019)	0.752 (1.016)	3.645 (3.543)	3.599 (3.511)	3.639 (3.546)	3.632 (3.529)
PBE0-D3/6-31G(d)	0.546 (0.757)	0.540 (0.770)	0.544 (0.763)	0.537 (0.747)	3.716 (3.607)	3.669 (3.565)	3.715 (3.614)	3.708 (3.596)
PBE0-D3/6-31+G(d,p)	0.523 (0.749)	0.518 (0.744)	0.521 (0.740)	0.514 (0.744)	3.727 (3.697)	3.680 (3.647)	3.733 (3.692)	3.720 (3.686)
PBE0-DCP/6-31+G(d,p)	(0.590)	(0.616)	(0.607)	(0.575)	(3.560)	(3.523)	(3.585)	(3.551)

The differences between the CP corrected values spans the 0.086 eV (for mM fit) ÷ 0.144 eV (for MS fit) energetic interval. Being well-known the adverse effect of BSSE, certainly, the CP-corrected D_e values should be considered as qualitatively binding energies for the two dimers.

^a Given parameters are obtained by fitting the calculated PECs to a modified-Morse (mM), Lennard-Jones (LJ), Murrell-Sorbie (MS) and Buckingham (B) potentials. Values obtained without CP correction are given in parentheses.

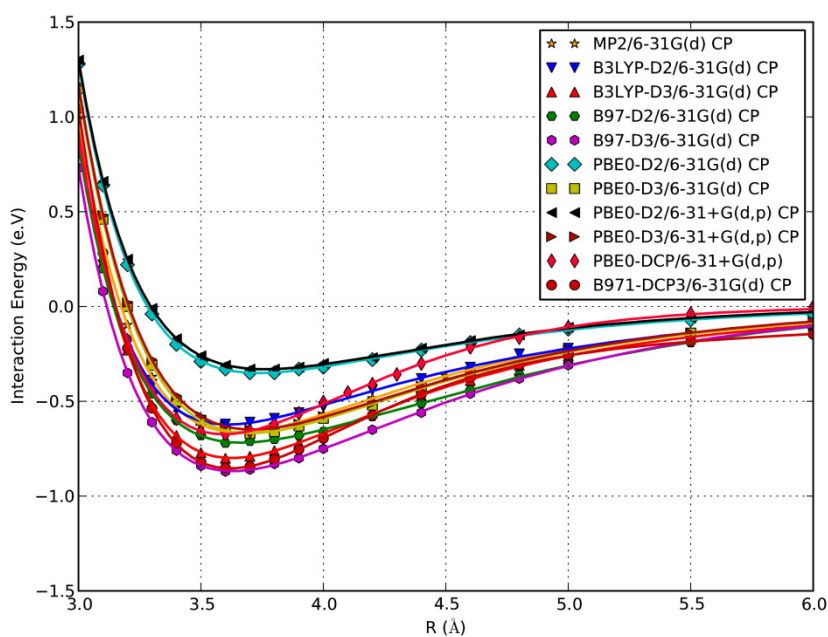


Fig. 4.2 Calculated potential energy curves for the stacked PTCDI dimer at different levels of theory, fitted to a Murrell-Sorbie potential function.

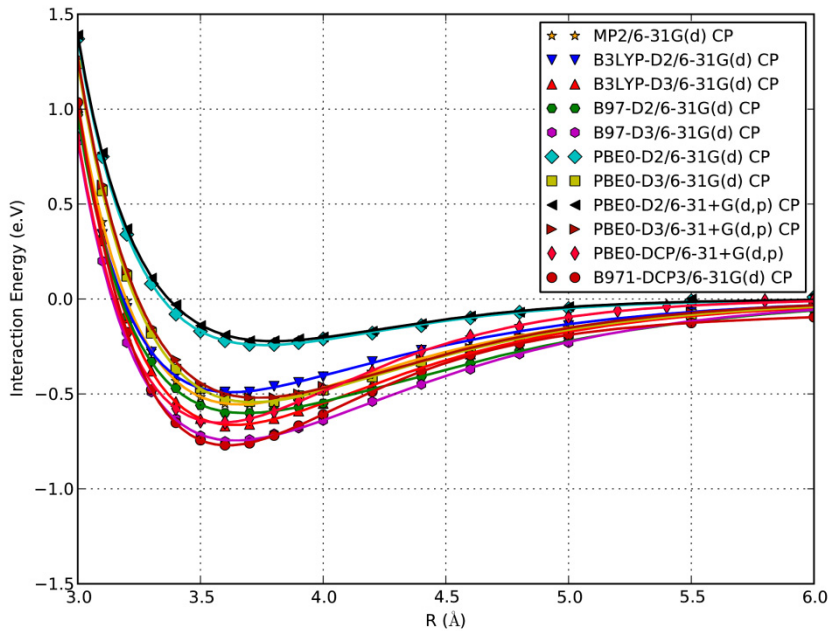


Fig. 4.3. Calculated potential energy curves for the stacked PTCDA dimer at different levels of theory, fitted to a Murrell-Sorbie potential function.

4.3 Impact of the dispersion correction scheme

As observed in Figures 4.2 and 4.3, the PBE0-D results are mostly affected by the adopted dispersion correction scheme. Thus, the PBE0-D3 binding energies are about 0.3 eV larger in magnitude, while R_e values are around 0.05 Å shorter than for PBE0-D2. On the other hand, the quality of the used basis sets does not affect considerably the PECs' parameters calculated by using these PBE0-D approaches.

The difference between the CP corrected D2 and D3 curves is nearly constant for the two used BSs. Thus, with BS2 $\Delta D_e = 0.318$ eV and $\Delta R_e = 0.053$ Å, while with BS1 the corresponding values are: $\Delta D_e = 0.317$ eV and $\Delta R_e = 0.039$ Å (stronger binding and smaller equilibrium distance offered by D3). Hence, going from D2 to D3 correction more binding energy is gained simultaneously with a shortening of R_e .

Depending on the binding energy ranges, for PTCDI, the PECs presented in

Fig. can be roughly divided into three categories. The first one includes the already discussed PBE0-D2 curves. The second category contains the MP2, B3LYP-D2/BS1, PBE0-D3/BS1, PBE0-D3/BS2, B97-D2/BS1 and PBE0-DCP/BS2 curves whose D_e values obtained from MS fit are between -0.718 and -0.623 eV. The third category includes B3LYP-D3/BS1, B97-D3/BS1 and B971-DCP3/BS1 curves with MS derived D_e values in the -0.868 ÷ -0.799 eV energy range.

4.4 Partial and full optimizations of the PTCDI and PTCDA dimers

Partially and fully optimized geometries of the PTCDI and PTCDA dimers given in

Fig. 4. were obtained at PBE0-DCP/BS2 level of theory, using different starting geometries and optimizing variables.

Expectedly, the fully optimized structures (FullOpt) are most stable, with binding energies of -1.294 eV and -1.098 eV for PTCDI and PTCDA, respectively. Hence, FullOpt PTCDI dimer is more stable than the PTCDA partner by 196 meV, a value which is about one order of magnitude greater than that obtained from the calculated PECs of the parallel eclipsed H-dimers.

FullOptX structures were obtained by the optimization of the dimers having as starting geometry the crystal structures.

A significant out-of-plane distortion of the monomers along one of their diagonal is noted for both fully optimized dimers, the difference in the Z coordinates of the O atoms on

one monomer diagonal and those of the O atoms on the other diagonal being almost equal (0.215 Å) for the two compounds. Even though the starting geometries were chosen so that the initial monomers were displaced and rotated to each other, however no significant displacement of the monomers to each other is observed in the fully optimized dimers, the differences in X and Y coordinates of the centers of the monomers being less than 0.001 Å for PTCDI and less than 0.005 Å for the PTCD A dimer.

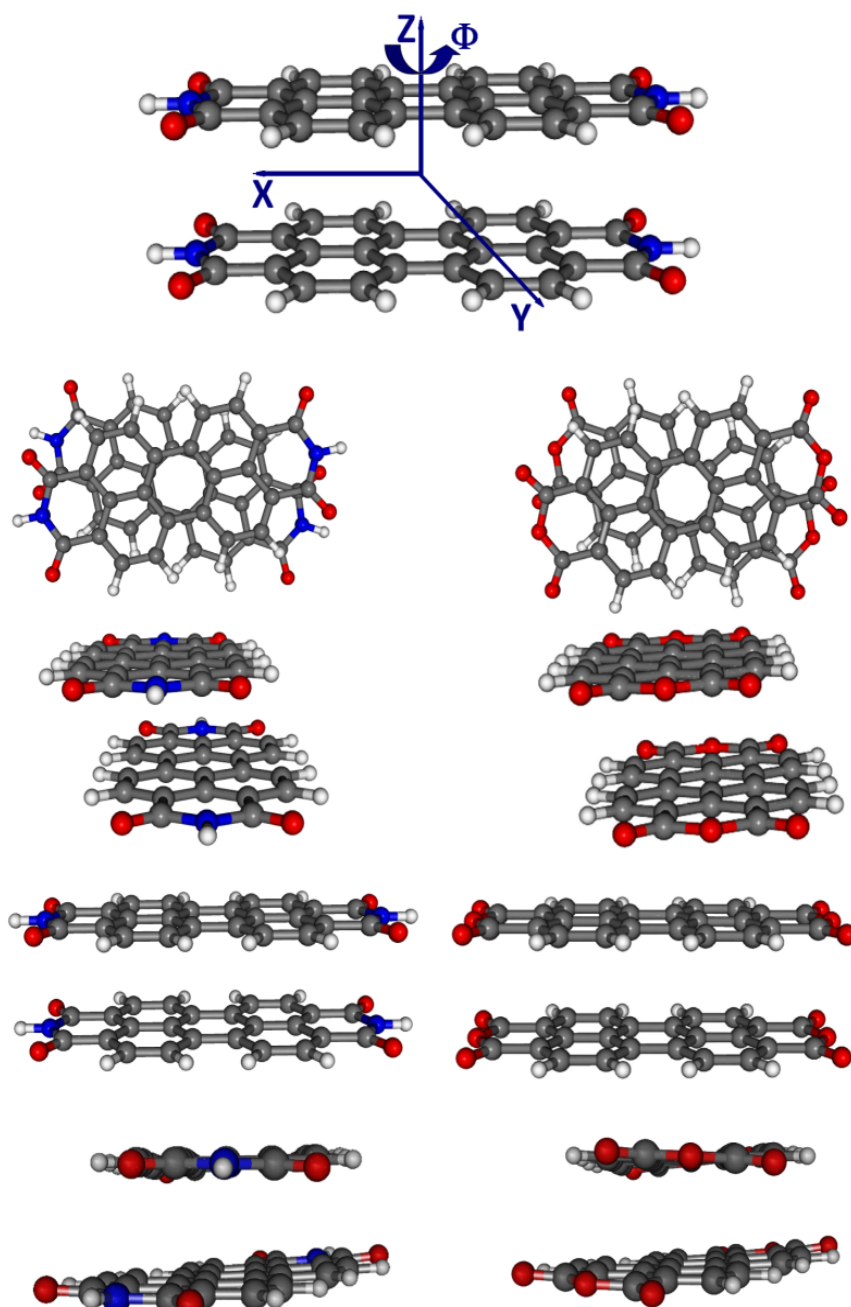


Fig. 4.4 Partially and fully optimized structures (from top to bottom: A, C, Parallel and FullOpt structures) of PTCDI (left) and PTCDAs (right) dimers calculated at PBE0-DCP/6-31+G(d,p) level of theory; the system of cartesian axes is shown on top.

4.5 Conclusions

In this work, post-Hartree-Fock (MP2) and density functional methods adapted for non-covalent interactions (DFT-D2, DFT-D3 and DFT-DCP) were applied to obtain the potential energy curves for the stacked dimers of PTCDI and PTCDAs perylene derivatives. Local minima as well as the global minimum on the potential energy surfaces of the two dimers have been obtained at PBE0-DCP/6-31+G(d,p) level of theory.

Dispersion energies are always larger in PTCDI dimer than in its PTCDAs partner and their order are reflected in the total interaction energies. While PBE0-D3 approach offers the smallest contribution of dispersion energy to the total interaction energy, for the two other used DFT-D methods this contribution is similar and it amounts around double the binding energy. Binding energies for all types of the investigated dimers is always larger for PTCDI than for PTCDAs.

Fully optimized structures of the two dimers at PBE0-DCP/BS2 level of theory correspond to twisted undisplaced monomers, mutually rotated by 30.1° and 31.4° for PTCDI and PTCDAs, respectively, with an important out-of-plane distortion of the composing monomers.

PBE0-DCP/6-31+G(d,p) approach was demonstrated as a pragmatic and computationally efficient quantum chemical method for calculating potential energy curves as well as for the scanning of potential energy surfaces and full optimization of large dimers as PTCDI and PTCDAs. Avoiding BSSE correction it provides PECs, binding energies and equilibrium distances in quantitative agreement with CP corrected MP2/6-31G(d) method.

Moreover, being different from the typical DFT-D approaches, the DFT-DCP method offers an independent analysis of the properties of two perylene dimers

5 Potential energy surfaces of TCNQ and 4F-TCNQ

5.1 Introduction

In spite of a numerous works published on the electronic structures of TCNQ and 4F-TCNQ, however, their potential surfaces have not been investigated in detail till now. For this reason, we used quantum chemical methods which are able to account for van der Waals interactions to investigate the potential energy surfaces of TCNQ and 4F-TCNQ [Mil11].

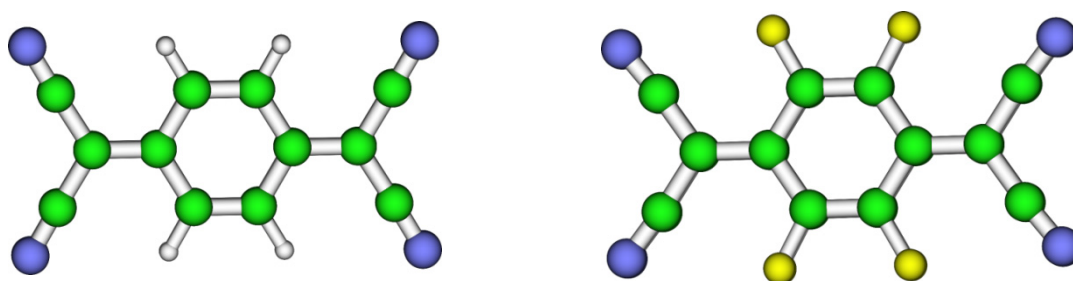


Fig. 5.1 Molecular structures of TCNQ (left) and 4F-TCNQ (right) monomers

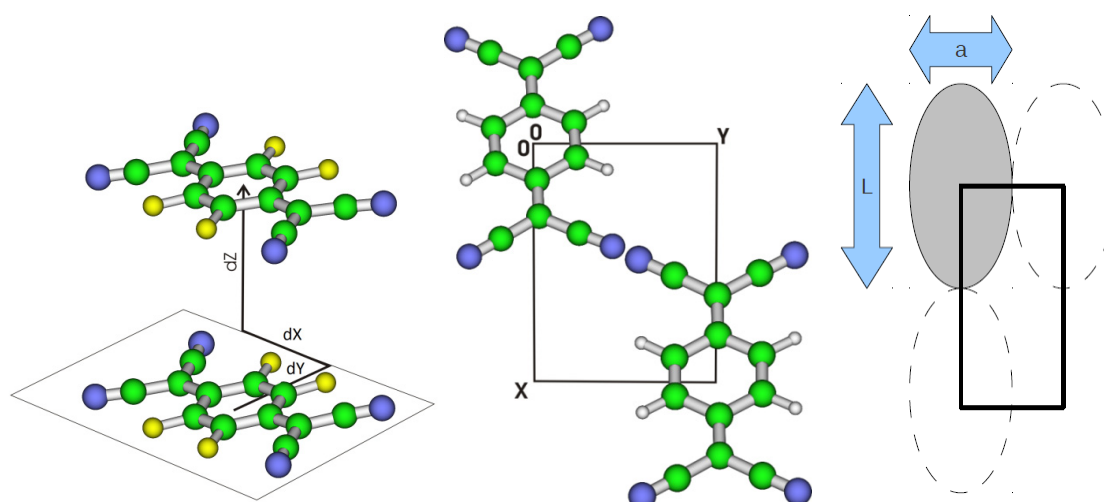


Fig. 5.2 Definition of the grid used for the calculation of the relaxed PES of TCNQ and 4F-TCNQ molecules.

5.2 Results and discussion

In this study we were interested to elaborate a protocol for locating the global minimum as well as local minima on the PES of the two investigated dimers. Such results

could be useful to understand the aggregation of these molecules in liquid phase and to explain their packing in solid state. Since for such non-polar molecules the self-assembling phenomena are largely governed by dispersive forces, the use of standard DFT methods is not recommended for this kind of studies. Instead we used the B3LYP functional in conjunction with the D2 dispersion corrected scheme proposed by Grimme [Gri06] which is already implemented in Gaussian program [Gau09]. First, we scanned the rigid PES of TCNQ to evaluate the possibility of this method in predicting this property and latter we scanned the relaxed PES of the two dimers. The scanned rigid PES of TCNQ is shown in Fig.5.3.

Local minima and the global minimum on the rigid PES of TCNQ and 4F-TCNQ dimers were obtained using their interplanar equilibrium distances obtained for the parallel stacked structures at the same level of theory (B3LYP-D2/6-31G(d)). For the TCNQ we used the $Z_{\text{fixed}} = 3.850 \text{ \AA}$ and for the 4F-TCNQ the Z_{fixed} was found to be 3.460 \AA .

For TCNQ a global minimum on the rigid PES is found at coordinates $\Delta X = 2.771 \text{ \AA}$ and $\Delta Y = 0.000 \text{ \AA}$, with an interaction energy of $E_{\text{int}} = -0.34 \text{ eV}$. Thus, the minimum energy for this dimer corresponds to a displaced structure along the long axis of the monomers. For 4F-TCNQ the global minimum on the rigid PES is found at $\Delta X = 3.500 \text{ \AA}$ and $\Delta Y = 1.455 \text{ \AA}$, with $E_{\text{int}} = -0.45 \text{ eV}$. In this case, significant displacements along the both X and Y axes lead to a minimum energy configuration.

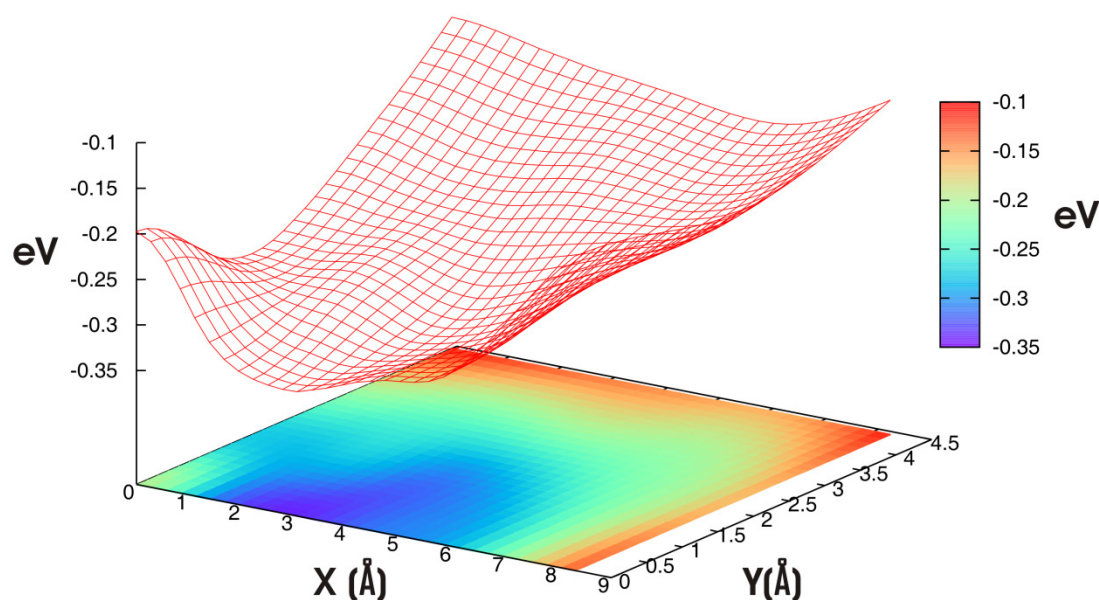


Fig. 5.3. Calculated rigid potential energy surface as a function of longitudinal (X) and transversal (Y) displacement with $Z_{\text{fixed}} = 3.850 \text{ \AA}$ for TCNQ dimer at B3LYP-D2/6-31G(d) level of theory.

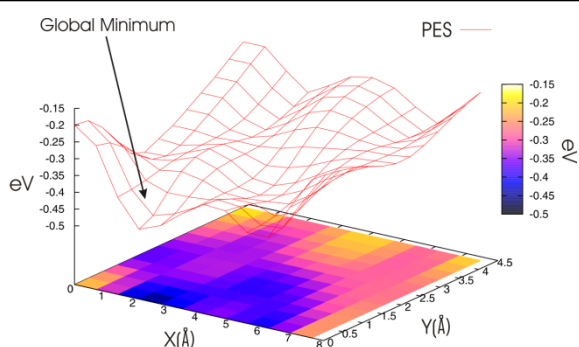


Fig. 5.4 Relaxed potential energy surface of TCNQ dimer calculated at B3LYP-D2/6-31G(d) level of theory.

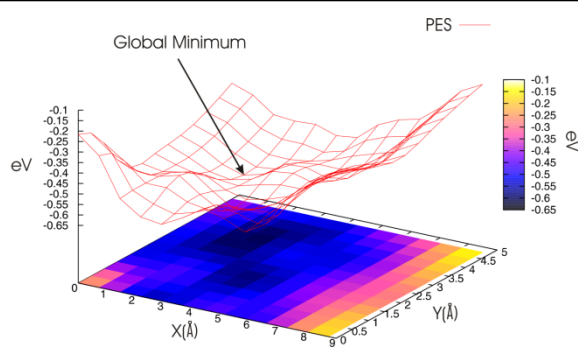


Fig. 5.5 Relaxed potential energy surface of 4F-TCNQ dimer calculated at B3LYP-D2/6-31G(d) level of theory.

Figures 5.4 and 5.5 show the relaxed potential energy surfaces obtained for the TCNQ and 4F-TCNQ dimers, respectively.

The global minimum obtained for the TCNQ relaxed PES has the coordinates: $\Delta x = 2.0779 \text{ \AA}$, $\Delta y = 0.0 \text{ \AA}$, $\Delta z = 3.182 \text{ \AA}$ and the equilibrium energy $E_{\text{min grid}} = -0.467 \text{ eV}$. In the case of the 4F-TCNQ molecule the minimum was found at the coordinates: $\Delta x = 2.183 \text{ \AA}$, $\Delta y = 3.583 \text{ \AA}$, $\Delta z = 2.911 \text{ \AA}$ and the equilibrium energy $E_{\text{min grid}} = -0.608 \text{ eV}$. The structure corresponding to the global minimum of the 4F-TCNQ dimer is strongly displaced along its long axis, the shift being roughly equal to that of half the width of such a ring. Concerning the vertical shift Δz , we observe that the inter monomer separation in case of relaxed PES is much lower than the value found by optimizing only this distance for the stacked dimer.

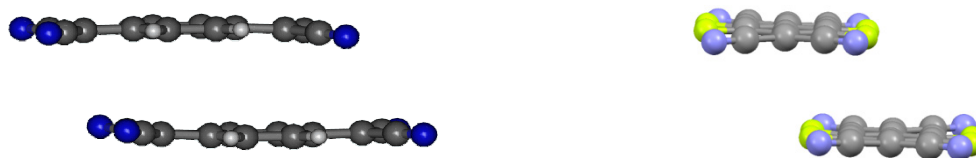


Fig. 5.6 Fully optimized structures of TCNQ (left) and 4F-TCNQ (right) dimers in gas-phase

The optimized inter-monomer geometrical parameters for the fully optimized TCNQ dimer $\Delta X = 2.100 \text{ \AA}$, $\Delta Y = 0.0 \text{ \AA}$ and $\Delta Z = 3.292 \text{ \AA}$. The difference between the geometry of the global minimum on the relaxed PES and the fully optimized structure are observed only for ΔX displacement and for the ΔZ . The monomer still remains undisplaced along its short molecular axis. For the 4F-TCNQ dimer, the fully optimized inter-monomer geometrical parameters ΔX , ΔY and ΔZ are 2.382 \AA , 3.261 \AA and 2.918 \AA respectively.

5.5 Conclusions

The rigid and relaxed potential energy surfaces of TCNQ and 4F-TCNQ dimers have been investigated at B3LYP-D2/6-31G(d) level of theory. For both dimers it is found that the

global minimum on the rigid PES is higher in energy than all the local minima found on the relaxed PES. Global minima on the relaxed PES are characterized by $D_e = -0.467$ eV for TCNQ and -0.608 eV for 4F-TCNQ. Different local minima identified for the two dimers are within 100 meV higher in energy than the global one.

While the global minimum for TCNQ has a structure displaced along the long axis of the molecule by 2.078 \AA , without any displacement along the Y axis, for 4F-TCNQ the global minimum of the relaxed PES corresponds to a structure displaced both on X (2.183 \AA) and Y (3.583 \AA) axes.

Fully optimized dimers have distorted geometries for monomers, with the CN groups pointing to the π -electron system of the partner monomer. Their energies are about 50 meV lower than those corresponding to the global minima on the relaxed PES.

Considering zero-point energy and BSSE effects, the upper estimates for the binding energies in the two fully optimized dimers are 300 meV and 400 meV for TCNQ and 4F-TCNQ respectively

General conclusions

A set of molecules (3,4,9,10-perylenetetracarboxylic diimide (PTCDI) and 3,4,9,10-perylenetetracarboxylic dianhydride (PTCDA), the molecular complex formed by one melamine and three PTCDI molecule, the 7,7,8,8-tetracyanoquinodimethane (TCNQ) molecule and its fluorinated 2,3,5,6-tetrafluoro-7,7,8,8-tetracyanoquinodimethane (4F-TCNQ) analogue) have been investigated by theoretical and experimental methods. We were interested in theoretical and spectroscopical characterization of these compounds which have interesting properties that make them suitable materials for applications in nanotechnology.

The molecular complex formed by a melamine and three PTCDI molecules is stabilized by three hydrogen bonds formed within each melamine-PTCDI pair. According to calculations, melamine-PTCDI complexes are more stabilized than the melamine-melamine or PTCDI-PTCDI monomers and melamine molecule has the ability to form stable complexes regardless of the number of PTCDI molecules. Moreover, the stabilization energy for the melamine-PTCDI complex is significantly greater than for the melamine-melamine or PTCDI-PTCDI dimers and thus, the preference for melamine-PTCDI interaction is expected, as found experimentally in a number of works.

The main features of the melamine-3PTCDI complex derived from the calculated IR spectrum are the vibrational bands related to hydrogen bonded groups, i.e. NH and CO from PTCDI and amino groups from melamine.

The absorption and fluorescence spectra of pure PTCDI compound were investigated in three different solvents (Chloroform, DMF and DMSO). Also, the ability of DFT-DCP methods for predicting the absorption and emission spectra of PTCDI were tested. Particular emphasis was put on the vibronic structure of its absorption and emission spectrum.

While clear evidences were observed for the aggregated PTCDI molecules in DMF and DMSO solvents, signal from such structures was not observed in chloroform solution. The methodology used in this study for the calculation of the excitation energies and vibronic structure of absorption and emission spectra can be routinely applied for other molecular systems.

Potential energy curves along the interplanar coordinate have been derived for the dimers of PTCDI and PTCEA molecules by using MP2 and dispersion corrected DFT methods with B3LYP, B97 and PBE0 density functionals. The performance of dispersion-correcting potentials for describing intermolecular van der Waals interactions was also tested in conjunction with PBE0 and B971 functionals. The calculated potential energy curves at different levels of theory have been fitted to a modified Morse, Murrell-Sorbie, Buckingham or Lennard-Jones potential and then the interaction energies and equilibrium distances were extracted.

The potential energy surfaces and potential energy curves for the dimers of TCNQ and its fluorinated derivative 4F-TCNQ were investigated by quantum chemical methods able to account for dispersion interactions, at B3LYP-D2/6-31G(d) level of theory. Global minima on the relaxed potential energy surfaces show that TCNQ dimer is less stable than the 4F-TCNQ partner by 145 meV. Moreover, the structures of the global minima in the two cases are completely different. Thus, TCNQ dimer has a displaced structure along the X axis without any shift on the short molecular axis, while the 4F-TCNQ dimer shows an optimized structure displaced both on X and Y axes.

Selected References

- Ant91 S. Antohe, N. Tomozeiu and S. Gogonea, *Phys. Status Solidi A*, 125 (1991) 397
- Aro97 R. Aroca, S. Rodriguez-Llorente, *J. Mol. Struct.*, 408-409 (1997) 17-22
- Aru93 E. Arunan, H. Gutowsky, *J. Chem. Phys.*, 98 (1993) 4294-4296
- Bal05 K. Balakrishnan, A. Datar, R. Oitker, H. Chen, J. Zuo, L. Zang, *J. Am. Chem. Soc.*, 2005, 127, 10496-10497
- Bal06 K. Balakrishnan, A. Datar, T. Naddo, J. Huang, R. Oitker, H. Chen, J. Zuo, L. Zang, *J. Am. Chem. Soc.*, 2006, 128, 7390-7398
- Chi09 V. Chiş, **G. Mile**, R. Ştiufiuc, N. Leopold, M. Oltean, *J. Mol. Struct.*, 924-926 (2009) 47-53
- Cla07 A.E. Clark, C. Qin, A.D.Q. Li, *J. Am. Chem. Soc.*, 129 (2007) 7586-7595.
- Dat06 A. Datar, R. Oitker, L. Zang, *Chem. Commun.*, (2006) 1649
- Fer06 A.J. Ferguson, T.S. Jones, *J. Phys. Chem. B* 110 (2006) 6891-6898.
- Gau09 Gaussian 09, Revision A.02, M. J. Frisch, G. W. Trucks, H. B. Schlegel, G. E. Scuseria, M. A. Robb, J. R. Cheeseman, G. Scalmani, V. Barone, B. Mennucci, G. A. Petersson, H. Nakatsuji, M. Caricato, X. Li, H. P. Hratchian, A. F. Izmaylov, J. Bloino, G. Zheng, J. L. Sonnenberg, M. Hada, M. Ehara, K. Toyota, R. Fukuda, J. Hasegawa, M. Ishida, T. Nakajima, Y. Honda, O. Kitao, H. Nakai, T. Vreven, J. A. Montgomery, Jr., J. E. Peralta, F. Ogliaro, M. Bearpark, J. J. Heyd, E. Brothers, K. N. Kudin, V. N. Staroverov, R. Kobayashi, J. Normand, K. Raghavachari, A. Rendell, J. C. Burant, S. S. Iyengar, J. Tomasi, M. Cossi, N. Rega, J. M. Millam, M. Klene, J. E. Knox, J. B. Cross, V. Bakken, C. Adamo, J. Jaramillo, R. Gomperts, R. E. Stratmann, O. Yazyev, A. J. Austin, R. Cammi, C. Pomelli, J. W. Ochterski, R. L. Martin, K. Morokuma, V. G. Zakrzewski, G. A. Voth, P. Salvador, J. J. Dannenberg, S. Dapprich, A. D. Daniels, O. Farkas, J. B. Foresman, J. V. Ortiz, J. Cioslowski, and D. J. Fox, Gaussian, Inc., Wallingford CT, 2009.
- Gri06 S. Grimme, *J. Comput. Chem.*, 27 (2006) 1787-1799.
- Gro87 J.R. Grover, E.A. Walters, E.T. Hiu, *J. Phys. Chem.* 91 (1987) 3233-3237.
- Gus97 K. Gustav, M. Leonhardt, H. Port, *Monatshefte für Chemie* 128 (1997) 105-112.
- Hau05 A. Hauschild, K. Karki, B.C.C. Cowie, M. Rohlfing, F.S. Tautz, M. Sokolowski, *Phys. Rev. Lett.*, 94 (2005) 036106.
- IUP97 IUPAC Compendium of Chemical Terminology, 2nd Edition, 1997.
- Kaa07 L.G. Kaake, Y. Zou, M.J. Panzer, C.D. Frisbie, X.-Y. Zhu, *J. Am. Chem. Soc.*, 129, (2007) 7824.
- Li06 X. Li, B. Xu, X. Xiao, X. Yang, L. Zang, N. Tao, *Faraday Discuss.*, 131 (2006) 111-120
- Lil06 O.A. von Lilienfeld, D. Andrienko, *J. Chem. Phys.*, 124 (2006) 054307.
- Llo98 S. Rodriguez-Llorente, R. Aroca, J. Duff, *J. Mater. Chem.*, 8 (1998) 629.
- Mil09 **G. Mile**, M. Oltean, V. Chiş, Potential Energy Surface of the Stacked PTCDI Dimer, International Conference on the Formation of Semiconductor Interfaces, Weimar, Germany, July 5-10, 2009, pag. 062.
- Mil11 **G. Mile**, M. Oltean, E. Meheş, N. Leopold, V. Chiş, Intermolecular potentials and potential energy surfaces of the TCNQ and 4F-TCNQ dimers calculated with MP2, DFT-D and DFT-DCP methods, International Conference on the Formation of Semiconductor Interfaces, Prague, Czech Republic, July 3-8, 2011.
- Mir11 N. E. Mircescu, **G. S. Mile**, M. Oltean, V. Chiş, N. Leopold, *Studia UBB Physica*, LVI, 1 (2011) 31-39.
- Olt11 M. Oltean, A. Calborean, M. Vidrighin, M. Iosin, **G. Mile**, L. Leopold, D. Maniu, N. Leopold, V. Chiş, Absorption and emission spectra of PTCDI: an experimental and TD-DFT investigation, Advanced Spectroscopies on Biomedical and Nanostructured Systems, September 4-7, 2011, Cluj-Napoca, Romania
- Olt12 M. Oltean, **G. Mile**, M. Vidrighin, N. Leopold, V. Chiş, *J. Comput. Chem.*, submitted
- Per06 L.M.A. Perdigo, E.W. Perkins, J. Ma, P.A. Staniec, B.L. Rogers, N.R. Champness, P.H. Beton, *J. Phys. Chem. B*, 110 (2006) 12539.

-
- Rui06 M. Ruiz-Oses, N. Gonzalez-Lakunza, I. Silanes, A. Gourdon, A. Arnau, J. E. Ortega, *J. Phys. Chem. B Lett.*, 110 (2006) 25573.
- Sal06 G. Salvan, S. Silaghi, M. Friedrich, C. Himcinschi, D.R.T. Zahn, *J. Opt. Adv. Mat.*, 8 (2006) 604.
- Sei06 J. Seibt, P. Marquetand, V. Engel, Z. Chen, V. Dehm, F. Wurthner, *Chem. Phys.*, 328 (2006) 354-362.
- Sil07 F. Silly, A.Q. Shaw, K. Porfyrakis, G.A.D. Briggs, M.R. Castell, *Appl. Phys. Lett.* 91(2007) 253109.
- Sil08 F. Silly, A.Q. Shaw, M.R. Castell, G.A.D. Briggs, *Chem. Commun.*, 2008, 1907-1909.
- Sin04 M.O. Sinnokrot, C.D. Sherrill, *J. Phys. Chem. A* 108 (2004) 10200-10207.
- Sto97 A. J. Stone, *The Theory of Intermolecular Forces*, Oxford University Press, Oxford, 1997.
- The03 J.A. Theobald, N.S. Oxtoby, M.A. Phillips, N.R. Champness, P.H. Beton, *Nature*, 424 (2003) 1029.
- Wan09 Y. Wang, H. Chen, H. Wu, X. Li, Y. Weng, *J. Am. Chem. Soc.*, 131 (2009) 30-31.
- Yan05 P. Yan, A. Chowdhury, M.W. Holman, D.M. Adams, *J. Phys. Chem. B*, 109 (2005) 724-730.
- Yan08 X. Yang, X. Xu, H.-F. Ji, *J. Phys. Chem. B*, 112 (2008) 7196-7202
- Zah04 D.R.T. Zahn, G. Salvan, B.A. Paez, R. Scholz, *J. Vac. Sci. Technol. A*, 22 (2004) 1482-1487
- Zha09 H.-M. Zhao, J. Pfister, V. Settels, M. Renz, M. Kaupp, V.C. Dehm, F. Wurthner, R.F. Fink, E. Engels, *J. Am. Chem. Soc.*, 131 (2009) 15660-15668.